JOURNAL OF MATERIALS SCIENCE 24 (1989) 1959–1966

Crack propagation in α-Al_2O_3/Mg metal matrix composites

A. MAGATA*, I. W. HALL
Department of Mechanical Engineering, and Centre for Composite Materials, University of Delaware, Newark, Delaware 19716, USA

The crack propagation characteristics of specimens of a unidirectionally reinforced α-Al_2O_3/Mg alloy metal matrix composite were investigated by means of fatigue crack propagation tests, tensile tests and fracture toughness tests. Samples were tested in longitudinal and transverse orientations. Fatigue crack propagation rates were successfully measured for each orientation. Crack propagation modes were found to be dependent upon the applied stress intensity and the fibre orientation. The crack propagation rates can vary by several orders of magnitude between nominally identical samples. In thermal cycling tests, voids were nucleated at the fibre/matrix interface: these voids decreased the load-carrying capability of the metal matrix composite but increased the work of fracture in the longitudinal orientation.

1. Introduction

Unidirectionally reinforced metal matrix composites (MMC) undeniably offer attractive tensile properties but their widespread acceptance and application depend upon two critical factors, namely, fabrication and crack propagation resistance. The objective of the present work was to focus upon the latter topic using a commercially available MMC system and to determine how the composite resisted crack propagation both under fatigue conditions and under rapid crack propagation conditions such as exist, for example, in a fracture toughness test.

Fatigue behaviour of unidirectionally reinforced MMC has been quite extensively studied, particularly for the older systems, such as B/Al [1–4]. In a study using beryllium and boron fibres in aluminium and aluminium alloy matrices, Hancock [1] concluded that crack branching at the fibre/matrix interface increased fatigue life and proposed that for good fatigue resistance the fibres should be brittle, the matrix should be ductile and have a low elastic modulus and that the interfacial bond strength should be low. A little differently, the shakedown model of Dvorak and Tarn [2] indicated that cyclic stresses occur in both the matrix and the fibres and that the composite would fail by matrix cracking if, as a result of this cycling, the stress in the matrix became larger than the fatigue limit of the matrix itself. The interface was not believed to play an important role but the stiffer the fibre and the higher the fatigue limit of the matrix then the better would be the fatigue life of the composite. Gouda *et al.* [3] observed that cracks formed early in the fatigue life at defects in the fibres in B/6061Al composites. In this work the fibre/matrix interface was found to play a very important role and two types of fracture occurred which were dominated by the strength of this interface. A weak interface led to debonding at the crack tip and caused the crack to spread up and down the interface in what was termed an "H"-type mode. A strong interface allowed little debonding and the crack propagated straight through the composite.

Considerable work has been carried out by Hack *et al.* [5–7] in systems incorporating α-Al_2O_3 fibres. They found the fatigue limit to vary between 0.6 and 0.95 of the tensile strength and to be strongly dependent upon the fibre volume fraction and orientation with respect to the loading axis. Rapid crack propagation has also been investigated for systems incorporating these and other fibres using fracture toughness tests.

However, the work to date on fatigue has generally suffered from the severe drawback that smooth specimens were used and attention has been directed towards the determination of fatigue life or strength which fails to distinguish between crack initiation and crack propagation and which also gives no information on crack propagation rates. The present report concerns the first successful attempt to generate fatigue crack propagation rate data for an α-Al_2O_3/Mg alloy MMC as a function of fibre orientation, along with fracture toughness values.

2. Experimental details

The material used in this study was FP™/Mg (E. I. DuPont de Nemours & Co. Ltd, Wilmington, Delaware). The matrix was ZE41A (Mg–4.2Zn–0.7Zr–1.2 rare earths), unidirectionally reinforced with 35 vol % α-Al_2O_3 fibres which are 20 μm in diameter. The composite was made by a vacuum infiltration technique, which has been reported elsewhere by Dhingra [8], and was supplied as plate 152 mm × 152 mm × 12.7 mm

Present address: Manufacturing Engineering Research Laboratory, Komatsu Ltd, 3-1-1 Ueno, Hirakata-shi, Osaka-Fu, 573 Japan.

0022–2461/89 $03.00 + .12

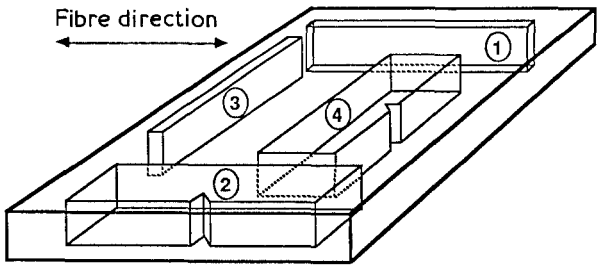

Figure 1 Designation of specimens with respect to original plate. 1, L orientation tensile specimen; 2, L orientation three-point bending specimen; 3, T orientation specimen; 4, T orientation three-point bending specimen.

from which tensile, fatigue and fracture toughness specimens were machined. Specimens were prepared in both the longitudinal, L, and transverse, T, orientations which are defined in Fig. 1.

Tensile specimens were 150 mm × 12.7 mm × 2.5 mm: the gauge length was 60 mm and aluminium end tabs were applied to the grips. Strain gauges were bonded to the centre of the gauge length and tests were performed at a strain rate of 2×10^{-2} min^{-1}. Stress/strain curves and Young's modulus values were calculated from data recorded on an Optilog recorder.

Crack propagation tests were performed using 60° notched three-point bend specimens 120 mm × 25.4 mm × 12.7 mm. Whenever possible, fracture toughness testing was performed according to ASTM standard E399 for metallic materials. In the L orientation, problems were encountered in producing fatigue pre-cracks and the following procedure was used. Crack opening displacement (COD) was monitored by use of a clip gauge and cyclic loading was applied at constant COD amplitude by use of the COD feedback signal. The load ratio, R, was set at 0.1 but as the crack grew the applied stress intensity, K, decreased and R also tended to zero. After crack growth had almost stopped the COD amplitude was increased and the crack propagated for a further distance before slowing down and stopping again. This procedure was repeated to produce a fatigue crack of the desired length and the sample was finally loaded monotonically to fracture in a fracture toughness test. For comparison purposes other fracture toughness specimens were prepared with a simple machined notch but without a fatigue pre-crack. Some fracture toughness tests were performed on samples which had been thermally cycled 30 times between two fluidized baths maintained at 400 and 25° C, respectively; each cycle consisted of 4 min in each bath.

Fatigue crack growth data were generated using the three-point bend samples described above containing either a simple notch or a chevron notch to aid in crack nucleation. In the T orientation, testing was performed exactly according to ASTM specification E647 at a frequency of 30 Hz and $R = 0.1$. The surface of the sample in the vicinity of the notch root was polished and lacquered; a reference grid was scribed in the lacquer and the crack length was monitored with a measuring microscope. In the L orientation, COD was again employed as the feedback signal and, as described above, had to be increased periodically during the test. The frequency used was 1.5 Hz and R was maintained at 0.2 because the machine could not be controlled at smaller values.

Fracture surfaces were examined in the scanning electron microscope and samples were prepared from selected specimens for examination in a Philips EM 400T transmission electron microscope (TEM). These samples were prepared by dimpling to $\sim 30\,\mu$m thickness and then ion milling to perforation at 3 keV on a cold stage.

3. Results

3.1. Tensile testing

Table I shows the average data from nine separate tests. Numbers in parentheses are the standard deviations and it can be seen that there is considerable scatter because the test pieces were taken from four different plates, each of which may have had slightly different processing parameters and slightly different volume fractions of fibres. The tensile strengths were consistently below the rule of mixtures (ROM) values calculated with the manufacturer's data. The average Young's modulus values coincided exactly for the longitudinal specimens and exceeded the ROM values for transverse specimens but the data are in broad agreement with tensile data from other studies [7, 9].

3.2. Fatigue crack growth tests

For the T orientation, fatigue crack growth rate, da/dN, was plotted as a function of ΔK, covering a range of 5×10^{-9} to 10^{-6} m/cycle: the data are shown in Fig. 2 and it is seen that the typical Paris Law equation

$$da/dN = C\Delta K^m$$

is obeyed quite well with an exponent, m, of 5 to 6.

For the L orientation, da/dN was plotted both as a function of ΔK and as a function of K_{max} because R decreased during the test. Fig. 3a shows da/dN plotted against ΔK for two separate specimens: the key shows the change in R in parentheses as initial and final R. Because the COD amplitude was increased three times during the test, three sets of experimental data were obtained for each specimen and are plotted in this figure. A poor and almost vertical straight line with considerable scatter could be drawn through the data, indicating that the crack propagation process does not closely follow the normal Paris equation.

Fig. 3b shows the da/dN plotted against K_{max} for the

TABLE I Tensile test data

Testing direction	UTS (MPa)	UTS/ROM	E (GPa)	E/ROM	ε_t	Poisson's ratio
Longitudinal	468(54)*	82%	161(16)*	100%	0.31	0.26
Transverse	131(28)	64%	88(12)	136%	0.21	0.31

*Numbers in parentheses represent one standard deviation.

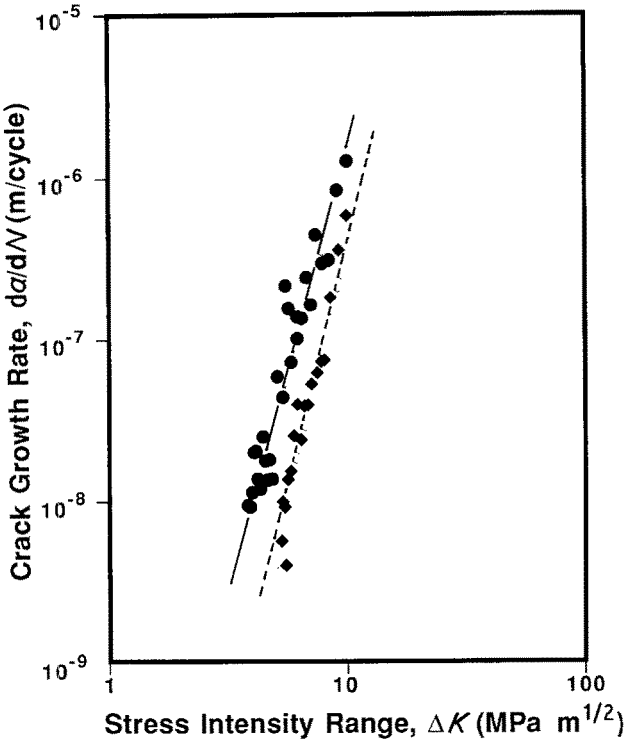

Figure 2 da/dN–ΔK data for T orientation. (●) Specimen 1, (◆) specimen 2. $R = 0.1, f = 30$ Hz.

same L samples. The data fall more closely on straight lines and the scatter, within each particular sample, is very small. The data, therefore, obey a modified Paris equation with an exponent of 16 to 18, which is very large compared with typical values for monolithic metals. However, the most striking observation is that, for the same value of K_{max}, the crack propagation rate varies from one plate to another over several orders of magnitude.

3.3. Fracture toughness testing

Fracture toughness tests, in both the longitudinal and transverse orientations, were performed on samples with fatigue pre-cracks and on others with simple machined notches. The data are presented in Table II; again the standard deviations are shown in parentheses. The fracture toughness in L orientation samples was ~ 18 MPa m$^{1/2}$, irrespective of whether a fatigue pre-crack was used or not. Similarly, in the T orientation the toughness was ~ 11 MPa m$^{1/2}$.

After the first series of tests and fractographic study, it became clear that there was little fibre pull-out, indicating a very strong fibre/matrix interfacial bond. In an attempt to weaken this bond, several samples from a single plate were subjected to thermal cycling as described above. The fracture toughness values were measured on samples with machined notches and all the relevant data from the tests are

TABLE II Fracture toughness data (MPa m$^{1/2}$)

Specimen	L orientation	T orientation
Fatigue pre-cracked	18.4 ± 2.6	10.0 ± 0.6
Machined notch	18.0 ± 2.7	11.6 ± 1.5

shown in Table III, including the area under the load–COD curve: P_{max} represents the maximum load and P_Q is the load used in calculation of the fracture toughness. This latter quantity is itself an alternative measure of the total work done in fracturing the sample, i.e. a measure of toughness. Using the normal ASTM 5% secant procedure for determining K_Q, the fracture toughness (or K_{IC} for a valid plane strain test), the values measured for these samples were inferior to those for uncycled specimens. However, the situation was radically different when the areas under the curves were considered and a 75% increase was noted for L orientation samples.

3.4. Fractography

Tensile fracture surfaces generally resembled the corresponding fast fracture regions of fracture toughness tests. Longitudinal specimens showed fracture surfaces consisting of a series of plateaux separated by cliffs about 30 μm high, each plateau corresponding to a region where a small bundle of fibres had failed in the same plane. Also, the individual fibres on each plateau had often debonded appreciably in the fracture toughness specimens and, although fibre pull-out was never extensive, there was clear evidence of plastic deformation because many fibres appeared to be situated in dimples and the matrix had necked down to a narrow ridge between fibres with a small amount of interface debonding (Fig. 4a). Transverse fracture surfaces showed bare and clean fibres and clean channels where fibres had been pulled out (Fig. 4b).

The fatigue fracture surface in the L orientation again consisted of plateaus, though the cliffs were now generally of smaller height. Between individual fibres on a plateau there was almost no evidence of plastic deformation and fibre debonding was practically absent (Fig. 5a). At the edges of the plateau, the magnesium matrix adhered to the fibres (Fig. 5b).

Fatigue fracture surfaces in the T orientation were very sensitive to the applied stress intensity range, ΔK. Figs 6a and b show the transition from failure predominantly through the matrix to fibre/matrix decohesion as ΔK increased from 4 to 10 MPa m$^{1/2}$. The static fracture mode of the fracture toughness test was clearly distinguishable from the fatigue pre-crack because of a sharp change in fracture mode. Fig. 7a shows the "ductile cleavage" fracture mode typical of fatigue to the left and the fibre/matrix interface fracture typical of static overload fracture to the right. The

TABLE III Fracture toughness data for uncycled and thermally cycled samples

Specimen	P_{max} (N)	P_Q (N)	P_{max}/P_Q	K_Q (MPa m$^{1/2}$)	Area (nm^2)
Longitudinal, uncycled	4350	4350	1	22.7	0.202
Longitudinal, cycled	3810	1720	2.22	9.1	0.354
Transverse, uncycled	2650	1300	2.03	6.8	0.18
Transverse, cycled	1690	700	2.41	3.7	0.12

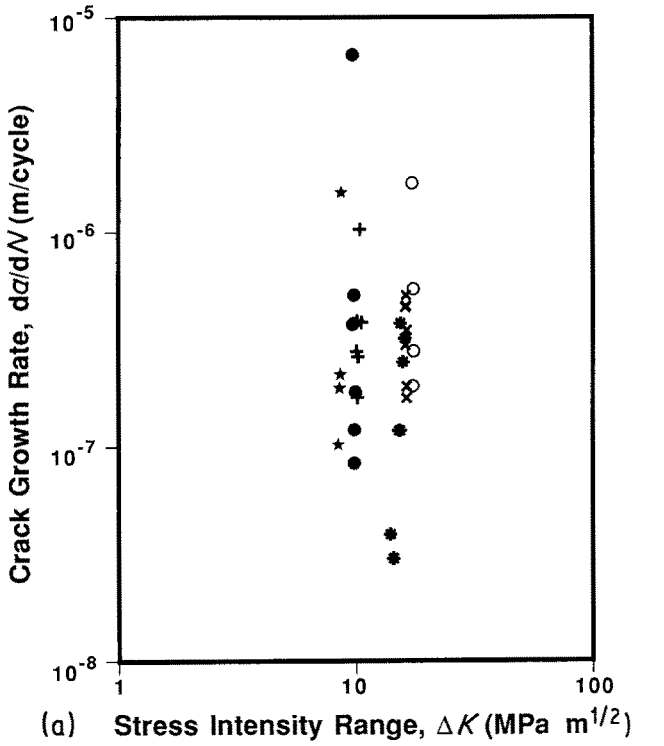

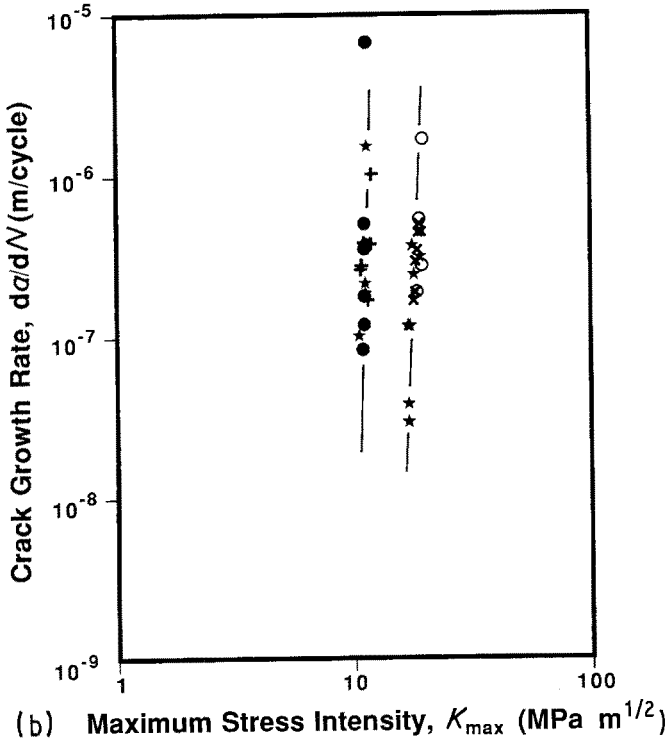

Figure 3 (a) da/dN–ΔK data for L orientation; (b) da/dN–K_{max} data for L orientation. $f = 1.5$ Hz.

Specimen 1			Specimen 2		
Expt.	Initial R → Final R		Expt.	Initial R → Final R	
1	●	(0.16 → 0.10)	1	○	(0.15 → 0.05)
2	+	(0.14 → 0.04)	2	×	(0.15 → 0.08)
3	★	(0.25 → 0.19)	3	✱	(0.18 → 0.06)

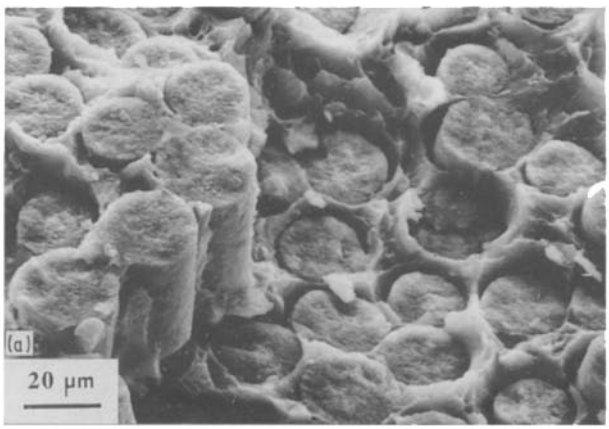

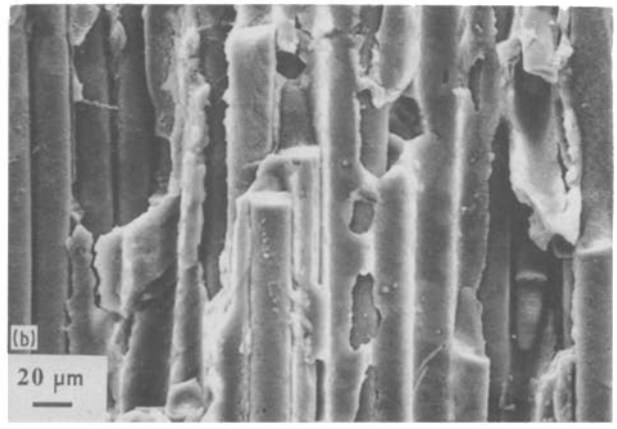

Figure 4 (a) Fractograph from L orientation tensile sample showing cliff, small amount of debonding and matrix ductility. (b) Fractograph from T orientation tensile sample showing predominantly fibre/matrix debonding.

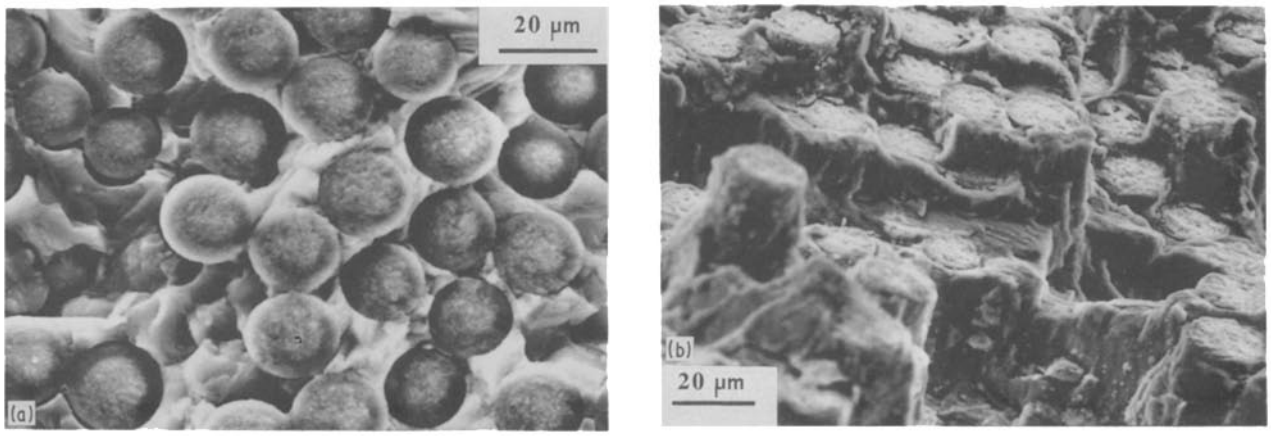

Figure 5 (a) Fatigue fracture of L orientation sample showing absence of both fibre debonding and gross plastic deformation. (b) Magnesium matrix adhering to fibres at edge of plateau.

higher magnification view of Fig. 7b shows this transition clearly with a fibre emerging from the matrix at the point where the fracture mode changes. Fracture toughness specimen surfaces in the T orientation, therefore, resembled the corresponding tensile fracture surfaces.

Thermally cycled L orientation fracture toughness specimens showed fracture surfaces which were qualitatively similar to uncycled ones but the plateau cliffs were much higher, the surface was macroscopically much rougher and fibre pull-out was rather more commonly observed. In the T orientation the surfaces resembled uncycled specimens except for the appearance of numerous small voids in the magnesium matrix between fibres (Fig. 8).

3.5. Metallography

Because the microstructures of these samples were similar to those reported previously for this material [10, 11], detailed metallographic study was limited to the thermally cycled samples and one as-fabricated sample, both from the same plate. Thermal cycling caused no changes in optical microstructure but did lead to clear differences in the TEM observations. Fig. 9 shows a micrograph of the fibre/matrix interface of an as-fabricated specimen in which the interfacial reaction layer is seen to be $\sim 0.1\,\mu m$ thick. The larger particles have been previously identified [11] and were confirmed to be MgO: the reaction layer also contains $MgO \cdot Al_2O_3$. When compared with a thermally cycled structure it is first observed that the MgO particles at the interface are considerably bigger and more frequent (Fig. 10a). Secondly, and perhaps most significantly, these samples showed a large number of small voids at the fibre/matrix interface. Some of these voids are indicated in Fig. 10a; Fig. 10b shows a higher magnification detail of two voids. These voids become much enlarged during the fracture process and give rise to the features seen on the fracture surface in Fig. 8.

4. Discussion

Beginning with the fatigue properties, the mechanical property data can be quite well rationalized in terms of the fractographic and microstructural observations reported above. Fatigue in the T orientation showed Paris law behaviour typical of monolithic metals, the only notable feature being the transition in crack propagation mode with increasing ΔK. At low ΔK values crack propagation is dominated by the properties of the matrix whereas at higher ΔK values the fibre/matrix interface begins to exert an influence. Calculating the plastic zone size from the equation [12]

$$r_c = 1/24\pi\,(\Delta K/\sigma_{ys})^2 \qquad (1)$$

gives a value which varies from 11 to 70 μm as ΔK increased during the test from 4 to 10 MPa $m^{1/2}$. With a mean centre to centre fibre spacing of 60 μm for this orientation it is clear that, at the lower ΔK values, K_{max} was insufficient to cause fibre/matrix decohesion but

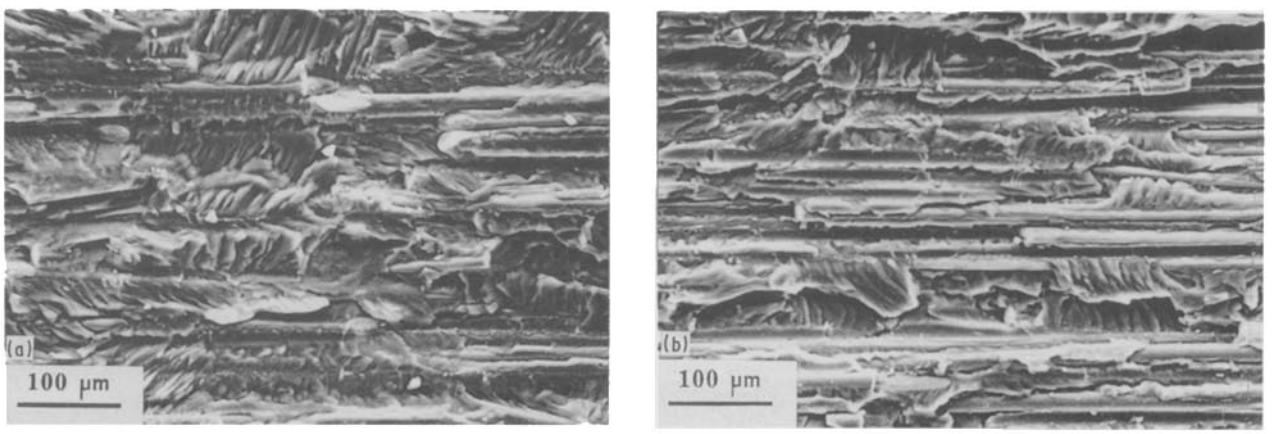

Figure 6 (a) T orientation: fatigue fracture surface produced with ΔK of ~ 5 MPa showing matrix-dominated fracture. (b) T orientation fatigue fracture at ΔK of ~ 8 MPa showing increased amount of fibre/matrix debonding.

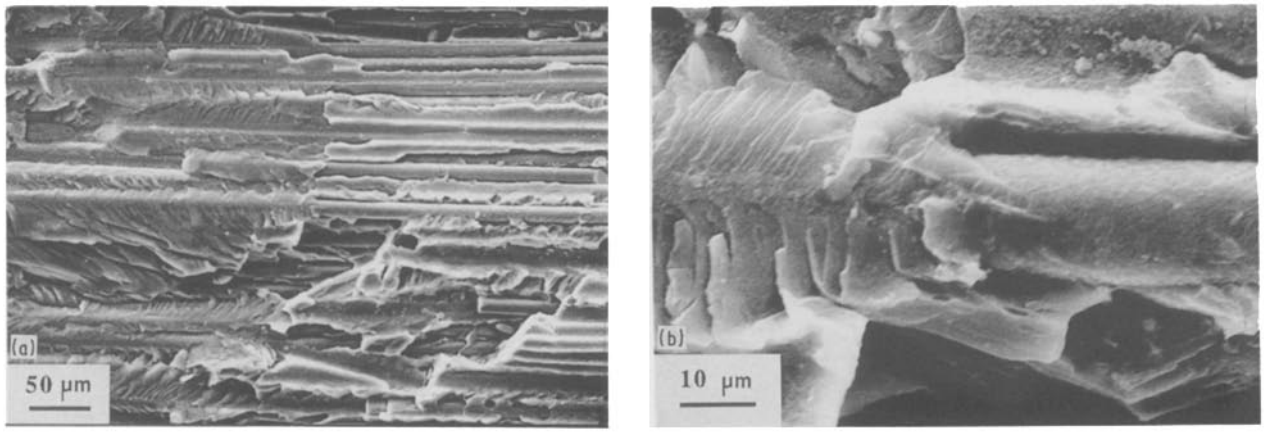

Figure 7 (a) Fatigue/final fracture transition in a T orientation sample, crack travelling from left to right. (b) Higher magnification of (a) showing transition from matrix to interface failure.

was large enough to cause plastic deformation and fatigue fracture of the matrix with the result that the plastic zone can be regarded as being confined to a region of the matrix between adjacent fibres. The transition towards fracture along the fibre/matrix interface occurred as ΔK increased during the test and the plastic zone enlarged to include some fibre/matrix interface regions and the two fracture modes became competitive.

There was no difference between the tensile test and the fracture toughness test fracture surfaces in the T orientation. Table II shows that the fracture toughness values were modest and were essentially independent of whether a fatigue pre-crack was present or not. This is further evidence that debonding and fracture occur when the stress intensity becomes large enough inside a plastic zone containing some fibre/matrix interface.

Turning to the L orientation samples, it was shown above that the Linear Elastic Fracture Mechanics (LEFM) concept of a plastic zone size had clear relevance to fatigue crack propagation in the T orientation: this is not so evident in the L orientation where, if the UTS of the composite is used in Equation 1, the plastic zone size can be calculated to vary up to 92 μm. However, under the isostrain conditions which may be assumed to apply, the stress in the matrix will be significantly less than this and the plastic zone size will be correspondingly smaller but does not immediately or obviously correspond to any microstructurally significant parameter. On close examination, however, the fractographic evidence did show a slight difference between rapid crack propagation and the slow fatigue crack propagation modes. Rapid crack propagation, as in a fracture toughness test, showed that the fracture surface contained plateaux where bundles of fibres had all failed in the same general plane and, presumably, in a related event. The edges of the plateaus contained exposed fibres indicating that they had joined up rapidly and at a sufficient stress intensity to cause fibre/matrix debonding. By contrast in the fatigue fracture surfaces, although the plateaux were still in evidence, the edges contained fibres which were covered by matrix indicating that link-up of these regions had occurred in a slower fashion by the advance of the ductile fatigue crack through the matrix in a manner similar to that for slow crack advance in the T orientation samples: compare Figs 5b and 4a. It may be concluded, therefore, that the fatigue crack did, in fact, propagate slowly and stably between plateau regions: this is in contrast to previous studies of fatigue in this material in which fatigue was concluded to have occurred by progressive random fibre fracture [9].

Fig. 3b shows fatigue data for two nominally identical samples in the L orientation in which the crack growth rate is seen to vary by more than three orders of magnitude, depending on the precise processing and microstructural conditions of the MMC. Such

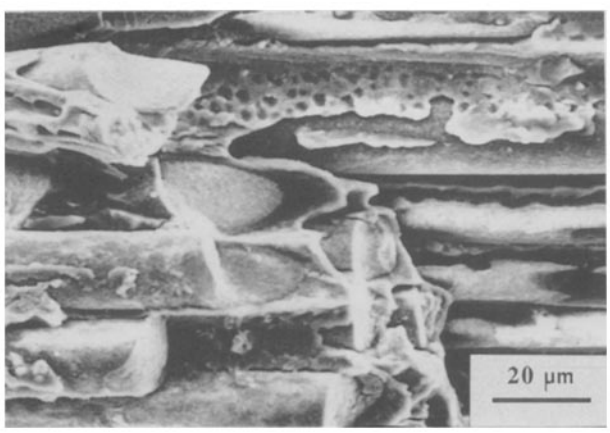

Figure 8 T orientation thermally cycled sample showing numerous voids at the fibre/matrix interface.

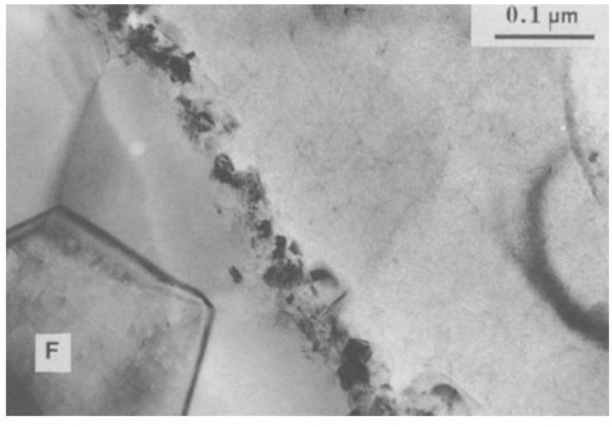

Figure 9 Transmission electron micrograph of as-fabricated sample showing narrow fibre/matrix interfacial reaction layer (fibre marked F).

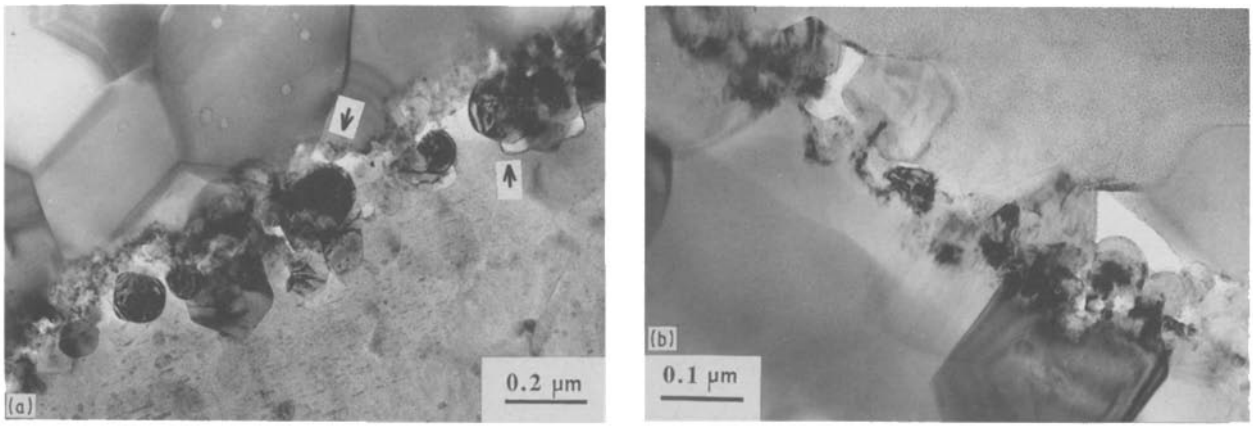

Figure 10 (a) Transmission electron micrograph of thermally cycled sample showing enhanced reaction at interface and several small voids (arrowed). (b) Higher magnification view of voids at interface.

variations in crack growth rates make these materials exceptionally sensitive to defects under fatigue conditions and slow, stable crack growth can occur at stress intensities much less than those necessary to cause rapid crack advance. These results indicate that crack growth can be expected to occur at stress intensities as low as $K_{IC}/2$. It is not yet clear which parameters are responsible for the variations in crack propagation rates but, as it is unlikely that a few per cent variation in volume fraction, V_f, or matrix strength would give this large effect, attention in future work will be focused upon the characteristics of the fibre/matrix interface.

On the other hand, Table II shows that the fracture toughness data are not sensitive to the presence of sharp cracks because samples with a machined notch gave values almost identical to those of fatigue precracked samples. Furthermore, even in samples which exhibited large variations in fatigue crack growth rate, the fracture toughness varied by only a small amount. This indicates that the fibre/matrix interface plays a different role in fracture toughness than in fatigue and indeed in fracture toughness situations energy is being expended in a large volume of material rather than very locally. The results from thermally cycled specimens dramatically confirm that this is the case.

TEM showed that thermal cycling produced incipient voids at the fibre/matrix interface as a result of the differing coefficients of thermal expansion of the matrix and the fibres. Although Table III shows that these voids reduced the total load-carrying capability of the interface and led to lower peak loads in the fracture toughness tests, it is seen that the total work done in fracturing the samples, as measured by the area under the load–COD curve, was increased by 75% in the L orientation. The voids caused a lowering of the fibre/matrix interfacial bond strength thus allowing debonding and enhanced crack deviation as was borne out by the fractographic evidence, see Fig. 8.

It may be argued that for many engineering applications the work of fracture is a more desirable measure of toughness and the material with a lower fibre/matrix bond strength is, therefore, preferable. In any event this work has shown that toughness is markedly affected by the fibre/matrix interfacial strength, the challenge now is to modify the surface condition to allow the development of optimum tensile properties whilst also allowing good toughness properties. This will certainly require a compromise because the former requires quite high bond strength whilst the latter requires rather low bond strength.

5. Conclusions

1. Fatigue crack growth rate data have been generated for FP™/Mg MMC in both the longitudinal and transverse orientations. Stable crack growth can be achieved even in the L orientation and the growth rate is described by a modified Paris equation.

2. In the T orientation, the fatigue crack growth process undergoes a transition from matrix failure to mixed matrix and fibre/matrix interface failure as ΔK increases.

3. In the L orientation, fatigue crack growth occurs by failure of fibre bundles and the subsequent joining up of these regions by fatigue cracking of the matrix.

4. Fracture toughness and strength are very dependent upon fibre/matrix bond strength but their requirements are conflicting.

5. Thermal cycling leads to void formation and coarsening of the MgO particles at the fibre/matrix interface.

Acknowledgements

The authors acknowledge the provision of the MMC used in this work by E. I. Du Pont de Nemours and Co. Ltd, Wilmington, Delaware. Financial support for one of us (A.M.) by Komatsu Ltd is also acknowledged.

References

1. J. R. HANCOCK, "Composite Materials: Testing and Design" (Second Conference), ASTM STP 497 (American Society for Testing and Materials, Philadelphia, Pennsylvania, 1972) p. 483.
2. G. J. DVORAK and J. Q. TARN, Fatigue of Composite Materials, ASTM STP 569 (American Society for Testing and Materials, Philadelphia, Pennsylvania, 1975) p. 145.
3. M. GOUDA, K. M. PREWO and A. J. McEVILY, "Fatigue of Fibrous Composite Materials", ASTM STP 723 (American Society for Testing and Materials, Philadelphia, Pennsylvania, 1981) p. 101.
4. J. R. HANCOCK and G. G. SHAW, "Composite Materials: Testing and Design" (Third Conference), ASTM STP 546 (American Society for Testing and Materials,

Philadelphia, Pennsylvania, 1974) p. 497.
5. K. S. CHAN, J. E. HACK and R. A. PAGE, *Met. Trans. A* **15A** (1984) 756.
6. J. E. HACK, R. A. PAGE and R. SHERMAN, *ibid.* **16A** (1985) 2069.
7. J. E. HACK, R. A. PAGE and G. R. LEVERANT, *ibid.* **15A** (1984) 1389.
8. A. K. DHINGRA, *Phil. Trans. Roy. Soc. Lond.* **A294** (1980) 559.
9. J. NUNES, E. S. C. CHIN, J. M. SLEPETZ and N. TSANGARAKIS, Proceedings of the International Conference on Composite Materials, V, edited by W. Harrigan (TMS, AIME, Warrendale, Pennsylvania, 1985) p. 723.
10. E. S. C. CHIN, US Army Materials Technical Laboratory Report MTL TR-87-7, Watertown, Mass. (1987).
11. R. A. PAGE, J. E. HACK, R. SHERMAN and G. R. LEVERANT, *Met. Trans. A* **15A** (1984) 1397.
12. J. R. RICE, "Fatigue Crack Propagation", ASTM STP 415 (American Society for Testing and Materials, Philadelphia, Pennsylvania, 1967) p. 247.

Received 7 April
and accepted 1 August 1988